Chapter 2
Seismological Implications of Fluid Effect on Earthquake Occurrence

Abstract It is becoming increasingly clear that pore fluids play an important role in a wide range of phenomena related to the generation of earthquakes and crustal deformation. Such view has been formed by combining results across diverse geophysical observations. Pore fluids will mainly fulfill a twofold role. One is purely mechanical one that occurs through fluid pressure change and the other is mechano-chemical effect such as stress corrosion cracking, pressure solution, and others. We put a focus on the effect of fluid pressure change here. In Sect. 2.1, we introduce the concept of Coulomb's law of friction coupled with the effective normal stress, which forms a basis for understanding mechanical effects of pore fluids on earthquake occurrence. In Sects. 2.2–2.9, we mention a variety of examples of seismological and geodetic observations that suggest the involvement of pore fluids in the generation of earthquakes. Finally in Sect. 2.10, we discuss a possibility to estimate hydraulic diffusivity of rocks forming fault zones on the basis of observation of seismic activity.

Keywords Aseismic slip · V_P/V_S value · Fluid flow · Induced seismicity

2.1 Effective Normal Stress and Coulomb's Law of Friction

It has become increasing clear over the past half a century that fluids, such as pressurized CO_2, magma, and water, have significant influence on earthquake occurrence. In fact, there exist observations that directly indicate the involvement of fluids in the occurrence of earthquakes such as earthquakes induced by reservoir impoundment and high-pressure fluid injection; see Sects. 2.4 and 2.5 below.

According to Coulomb's law of friction, the resistance to slip on an interface is described by the coefficient of friction, defined as the ratio of shear frictional stress to the normal stress acting on the interface, required to initiate slip (the coefficient of

T. Yamashita and A. Tsutsumi, *Involvement of Fluids in Earthquake Ruptures*,
DOI 10.1007/978-4-431-56562-8_2

static friction) or maintain slip (the coefficient of sliding friction). In other words, the shear frictional stress τ_s is related to the normal stress in a form

$$\tau_s = -\mu(\sigma_n^0 + \sigma_n) \tag{2.1}$$

on a frictional interface if no fluids are present and cohesion is negligible, where μ is the coefficient of friction, which takes values $\mu = \mu_{stat}$ and $= \mu_{slid}$ $(\mu_{stat} > \mu_{slid})$ at the onset of slip and during the slip, respectively. Here, σ_n denotes a change of the normal stress acting on the interface from some reference state prior to the slip onset, and the superscript or subscript 0 denotes a quantity at the reference state throughout the present book. We assume in this chapter, and Chaps. 4–6 that the normal stress is negative for compression and the fluid pressure is positive for compression, which is the usual convention in continuum mechanics. We also assume a compressive tectonic stress regime, so that σ_n^0 in (2.1) should be negative. Equation (2.1) is one of the simplest friction laws and is generally referred to as Coulomb's law of friction when μ_{stat} and μ_{slid} are constants. If we consider slip in rocks permeated with pore fluid, we will have

$$\tau_s = -\mu\sigma_{eff}^n, \tag{2.2}$$

replacing the normal stress $\sigma_n^0 + \sigma_n$ by an effective normal stress σ_{eff}^n. The effective normal stress can be written as $\sigma_{eff}^n = \sigma_n + \sigma_n^0 + a(p_f^0 + p_f)$ in a linear theory since the fluid pressure does not affect the shear stress, where p_f is the fluid pressure change from a reference state p_f^0 and a is a constant related to frictional property and/or poroelastic property of fault rocks. Although there exist studies to derive the expression for parameter a theoretically [see Sect. 7.5 of Paterson and Wong (2005)], laboratory experiments show that the relation $a = 1$ is approximately valid for fracture and friction strengths of many types of rocks including rocks with clay fault gouges at least for relatively slow slips (e.g., Brace 1972; Morrow et al. 2002). We assume $a = 1$ below when the concept of effective normal stress is applied. The above consideration indicates that (2.1) should be replaced by

$$\tau_s = -\mu(\sigma_n^0 + p_f^0 + \sigma_n + p_f) \tag{2.3}$$

when the fault zone is permeated with pore fluid. Hubbert and Rubey (1959) first applied the concept of effective normal stress to the problem of faulting.

Equation (2.3) points out that the elevation of pore fluid pressure can induce fault slip if high-pressure fluid is present, and there is some mechanism to raise the fluid pressure. Some examples of seismological and geodetic observations are given below in this chapter that suggest the existence of high-pressure fluids in seismogenic zones. We will also show examples strongly suggesting that high-pressure fluids affect earthquake occurrence.

2.2 Low P- and S-Wave Velocities and High V_p/V_s Values as an Indicator of the Presence of High-Pressure Fluid

It is known that the ratio of P- to S-wave velocities (V_p/V_s) for common rock types generally has values between 1.7 and 1.9 (e.g., Christensen 1996). However, P- and S-wave velocities and V_p/V_s value are known to vary with pore fluid pressure. In fact, Christensen (1984) found increase in Poisson's ratio $(= (1/2)\left[(V_p/V_s)^2 - 2\right]/\left[(V_p/V_s)^2 - 1\right])$ and decrease in P- and S-wave velocities with increasing pore fluid pressure at constant confining pressure by measuring P- and S-wave velocities under water-saturated condition for oceanic basalt and dolerite. This suggests that increasing pore fluid pressure has a greater effect on S-wave velocities than P-wave velocities under water-saturated condition. Hence, zones of high V_p/V_s values (or high Poisson's ratios) are generally interpreted as evidence for the presence of overpressured fluid if such zones are also characterized by low V_p and V_s values (e.g., Eberhart-Phillips and Michael 1993; Dawson et al. 1999; Nakajima et al. 2001; Matsubara et al. 2009). Zones characterized by high V_p/V_s values and low V_p and V_s values are sometimes observed beneath volcano calderas, which are attributed to the presence of partial melt (e.g., Dawson et al. 1999; Waite et al. 2006). Such zones have also been found near the upper boundary of subducting oceanic slab (e.g., Kamiya and Kobayashi 2000; Matsubara et al. 2009; Moreno et al. 2014). For example, Peacock et al. (2011) observed a zone of anomalously high V_p/V_s values about 2.35 along a landward dipping layer at the Cascadia subduction zone. They attributed the high V_p/V_s values to the presence of pore fluid near lithostatic pressure with a porosity of 2.7–4.0%. Moreno et al. (2014) found, analyzing seismological data, the spatial variation of V_p/V_s values around the interface of subducting oceanic slab ruptured during the 2010 M_w8.8 Maule, Chile, earthquake. They also found that high V_p/V_s domains correlate spatially with parts of the plate interface that are poorly locked and slip aseismically. Low V_p/V_s domains were shown to correlate with locked parts of the plate interface, where earthquakes are expected to occur. This finding suggests that variations in pore fluid pressure at plate interface control the interseismic locking. Hence, revealing V_p/V_s values and P- and S-wave velocities may be a key for understanding the mechanical properties of plate interfaces.

We can mention dehydration reaction and seawater trapped immediately before the subduction of oceanic slab as origins of high-pressure pore fluid that give rise to low P- and S-wave velocities and high V_p/V_s values at subduction slab interfaces. For example, it has been proposed that subducted oceanic lithosphere is dehydrated with increasing pressures and raising temperatures (e.g., Peacock 1996). Dehydration may be closely related to the occurrence of intermediate-depth earthquakes. Seno et al. (2001) actually tried to understand the seismicity in the Philippine Sea slab subducting beneath southwest Japan on the basis of dehydration embrittlement. Seno (2009) estimated the values of p_f^0/σ_n^0 acting on various interplate megathrusts and attributed their variation to the difference in the degree of

dehydration reaction. See Sect. 1.2 concerning recent geological knowledge on the sources of fluids in subduction zones.

Low V_p and V_s values and high V_p/V_s values have also been observed near hypocenters of large crustal intraplate earthquakes. For example, Zhao et al. (1996) found such features near the hypocenter of the 1995 M_w6.9 Hyogo-ken Nanbu (Kobe), Japan, earthquake. They attributed them to overpressurized, fluid-filled, fractured rock matrix, which is consistent with numerous evidences from hydrological, geochemical, and geophysical investigations about the above earthquake (Zhao and Negishi 1998). Potential sources of such fluid may be meteoric water or slab dehydration as mentioned by them.

Zones of anomalously low V_p/V_s values are also sometimes reported near earthquake hypocenters, and several mechanisms have been proposed for the existence of such zones. For example, Kurashimo and Hirata (2004) found a low-velocity zone with low-to-moderate values of V_p/V_s beneath the northern Fossa Magna basin, central Japan. Kato et al. (2010a) observed earthquake swarm in a zone with low V_p and anomalously low V_p/V_s values. Both Kurashimo and Hirata (2004) and Kato et al. (2010a) attributed such features of velocity structure to the presence of fluid-filled pores with high-aspect ratio on the basis of the analysis of Takei (2002), who theoretically studied the role of fluid compressibility and pore geometry on the V_p/V_s ratio. Hacker and Abers (2012) suggested that V_p/V_s value of $\sim$1.65 observed in several subduction-zone mantle wedges can be explained by the velocity anisotropy of peridotite with oriented minerals.

In closing this section, we will have to emphasize that V_p/V_s values and P- and S-wave velocities are affected by many other factors such as rock type, porosity, pore geometry, SiO_2 content, in situ stress, fluid compressibility, and temperature (e.g., Eberhart-Phillips et al. 1995; Christensen 1996; Takei 2000, 2002).

2.3 Change of P- and S-Wave Velocities of Fault Zone Before and After the Occurrence of Earthquake

Some seismological analyses have reported postseismic increase of P- and S-wave velocities in fault zones (e.g., Vidale and Li 2003; Peng and Ben-Zion 2006). For example, Vidale and Li (2003) monitored seismic wave velocity change of the shallow Johnson Valley fault zone after its rupture in the 1992 M_w7.3 Landers, California, earthquake. They found a consistent velocity increase over time across their 1994, 1996, 1997, and 1998 surveys. They interpreted the velocity increase in terms of the degree of fluid saturation in microcracks in the fault zone on the basis of the theoretical study of Garbin and Knopoff (1975), who analyzed the overall elastic moduli of medium permeated by isotropically oriented penny-shaped cracks. Vidale and Li (2003) found that the fluid saturation rose from 60 to 80%, which may be caused by the flow of groundwater into microcracks that opened in the Landers earthquake in combination with diminishing crack pore volume.

In contrast to the postseismic changes, coseismic deformation has been reported to cause decreases in the seismic wave velocities. Li et al. (2006) investigated, using aftershocks and artificial explosion, seismic wave velocity change in the San Andreas fault zone before and after the 2004 M_w6.0 Parkfield, California, earthquake. They found the decrease of S-wave velocity of fault zone by 1.25% in a time period between October 2002 and 3 months after the mainshock, which is likely due to sudden microcrack generation induced by the dynamic slip and strong ground shaking. The former and latter are generally referred to as slip-induced dilatancy and shaking-induced dilatancy, respectively, both of which can decrease the degree of fluid saturation; see Sect. 4.10 as to the concept of slip-induced dilatancy. Li et al. (2006) interpreted the observed coseismic velocity decrease within the fault zone as mainly due to the slip-induced dilatancy caused by the mainshock. Li et al. (2006) also found tendency of increase of S-wave velocity in the postseismic period as observed by Vidale and Li (2003).

Changes of the V_p/V_s values are also observed for earthquake swarms. Dahm and Fischer (2013) estimated V_p/V_s values during the 1997, 2000, and 2008 swarms in Western Bohemia, central Europe. They found a strong temporal decrease of V_p/V_s values for all swarms before and during the main activity of each swarm; V_p/V_s values recovered to background levels at the end of the swarms. Since earthquake swarms seem to be closely related to the presence of high-pressure fluid as will be described in Sect. 2.8, such change in V_p/V_s values may reflect the change in pore fluid properties.

2.4 Reservoir-Induced Seismicity

Earthquake occurrence rates have been reported to increase after filling newly constructed water reservoirs in their vicinity (e.g., Carder 1945; Gupta and Rastogi 1976; Gupta 1992, 2002). Carder (1945) reported the occurrence of several hundred felt earthquakes in the vicinity of Lake Mead, Nevada-Arizona, after filling it in the late 1930s. Since the identification of causal association of seismicity with the lake impoundment by Carder (1945), numerous reports have been given about reservoir-induced seismicity. Well-known early examples will be earthquakes occurred in the 1960s at Hsinfengkiang, China, Kremasta, Greece, and Koyna, India (Simpson 1986; Gupta 2002). Although the events occurred near Lake Mead were of low magnitudes and did not cause any damage, relatively large damage-causing events sometimes occur in other areas (Narain and Gupta 1968). One of such examples will be events occurred near the Koyna Dam in a region of India, which had been considered to be stable and nonseismic (Lee and Raleigh 1969). Small-size events began to occur near the dam site soon after the impoundment of the Koyna Dam reservoir in 1962 and the frequency of events increased considerably from mid-1963 (Narain and Gupta 1968). In 1967, an earthquake of M_w6.3 eventually occurred near the dam site and caused about 200 deaths and 1500

injuries in the nearby town (Gupta and Rastogi 1976; Gupta 2002). A series of events occurred near the Koyna Dam support the idea that the earthquakes were affected by the impoundment of reservoir. Davies et al. (2013) compiled a list of 39 possible examples of reservoir-induced earthquakes.

Two independent effects may be considered as the effect of reservoir impoundment (e.g., Simpson 1986). One will be the influence of elastic reservoir loading; the loading increases with the impoundment. The other will be the influence of pore fluid pressure; pore fluid will diffuse from the reservoir into the surrounding media, which can change the pore fluid pressure distribution in the vicinity of the reservoir. The former can raise the shear traction acting on preexisting faults, whereas the latter can decrease the effective normal stress acting there. Both can promote slip on nearby preexisting faults.

2.5 Seismicity Induced by the Injection of High-Pressure Fluid

Increase in seismicity is known to result from the injection of high-pressure fluid into the ground (Simpson 1986; Ellsworth 2013). If we are interested only in understanding the effect of pore fluid on earthquake faulting, it may be much advantageous to consider the injection of high-pressure fluid into deep wells because the injected fluid mass is relatively small and cannot change the elastic stress state substantially. In other words, we can extract only the effect of pore fluid pressure change.

Earthquakes induced by the injection of high-pressure fluid were first reported for earthquakes that occurred near Denver, Colorado, between 1962 and 1967 (Evans 1966; Healy et al. 1968). A 3671-m-deep disposal well was completed in 1961 to pump contaminated waste fluid into the ground at the Rocky Mountain Arsenal at northeast of Denver. The injection began in March 1962 and continued through September 30, 1963, at an average rate of about 21 million L per month. Since the start of fluid injection, a large number of earthquakes had been recorded. At the end of September 1963, the injection well was shut down and no fluid was injected until operations were resumed on September 17, 1964. During the period from April 1962 to the end of September 1965, 710 earthquakes were recorded with epicenters in the vicinity of the Arsenal. Figure 2.1 illustrates the monthly volume of waste injected into the well and the monthly number of earthquakes. The majority of earthquake epicenters were within an 8 km radius of the well. Evans (1966) pointed out that high injection rate months April, May, and June 1962 correlate with the high earthquake frequency months of June, July, and August (filled in black in Fig. 2.1). The high injection rate months of February and March 1963 seem to correlate with the high earthquake frequency month of April (filled in black in Fig. 2.1). In addition, the period of no-injection from September 1963 to

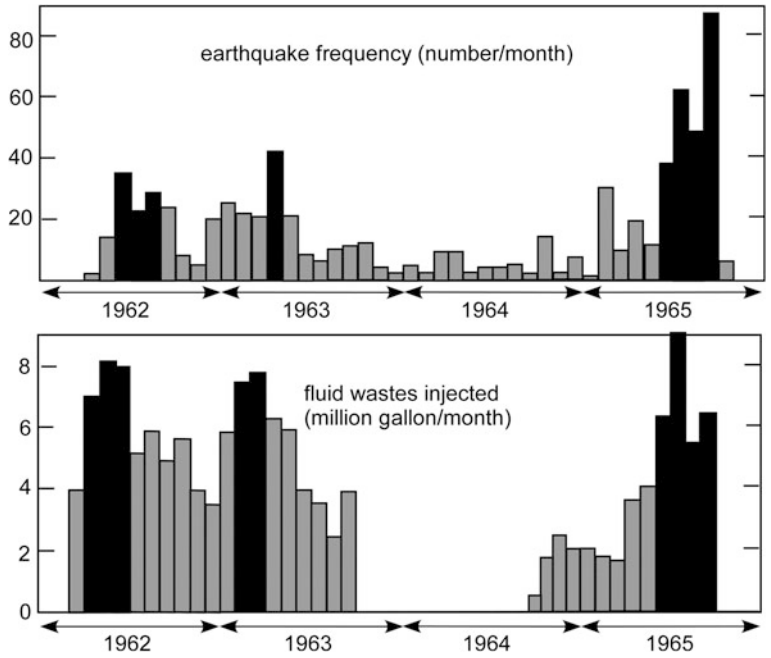

Fig. 2.1 Monthly volume of waste fluid injected into the well and monthly number of earthquakes occurred in Denver area; 1 gallon = 3.78 L. Modified from Evans (1966), reprinted with the permission from the Rocky Mountain Association of Geologists

September 1964 coincides with a period of minimum earthquake frequency. We also observe a strong correlation between June and September 1965 (filled in black in Fig. 2.1).

To test the hypothesis of effective normal stress in a field, Raleigh et al. (1976) carried out a field experiment using 2000-m-deep wells at the Rangely oil field, Colorado, which had been on waterflood for secondary oil recovery since 1957. They estimated a critical pore fluid pressure of 25.7 MPa from laboratory measurement of static friction coefficient of core samples of the reservoir rocks and in situ measurement of stress state at the depth of earthquake hypocenters. They conducted fluid injection as well as fluid withdrawal experiments using four experimental wells between 1969 and 1973 to examine the correlation between the fluid pressure change and seismicity. They found a significant increase in the seismicity near the experimental wells when the fluid pressure in the monitoring well exceeded the critical pressure 25.7 MPa, which suggests the validity of the concept of effective normal stress. They also found a sudden decrease in seismicity soon after the start of backflow in 1973.

Similar field experiments were conducted at other locations. Experiment on fluid-induced seismicity was made at Matsushiro, central Japan, in 1970 (Ohtake 1974). Water amounting to 2883 m^3 was pumped into a 1800-m-deep well, and

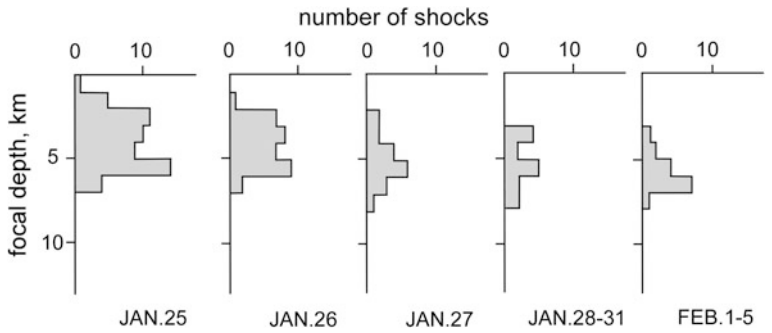

Fig. 2.2 Spatiotemporal change of hypocenter depths during the water injection at Matsushiro, Japan. The injection started on January 15, 1970. Modified from Ohtake (1974), reprinted with the permission from M. Ohtake

seismicity of Matsushiro area was monitored. He found the occurrence of microearthquakes nine days after the start of injection and slow downward migration of hypocenters (Fig. 2.2) along the fault slipped during the Matsushiro swarm earthquakes started in August of 1965. Although this is commonly interpreted as being due to the flow of water along the fault, we cannot deny a possibility of occurrence of aseismic slip coupled with fluid flow according to recent studies at other areas (e.g., Scotti and Cornet 1994) as will be described below in this section.

In 1997, pressurized water was injected into a 1800-m-deep borehole drilled to the southern end of the surface trace of the Nojima fault that slipped during the mainshock of the 1995 M_w6.9 Hyogo-ken Nanbu (Kobe), Japan, earthquake (Tadokoro et al. 2000). They found an increase in seismic activity four to five days after the start of water injection; slow migration of hypocenters with speeds 2–40 m/h was also observed. They interpreted the induced earthquakes as events occurred inside the fault zone. Zoback and Harjes (1997) studied earthquakes induced by the injection of KBr/KCl brine into a much deeper borehole of depth 9.1 km in Germany. They found a large number of microearthquakes induced around the depth of 8.8 km. It was also found that many of the earthquakes were induced by extremely low fluid pressure perturbations (<1 MPa), which suggest that the crustal stress was near a critical level. Although determined hypocenters of induced seismicity give only a blurry image of rupture evolution in former studies, Rutledge and Phillips (2003) and Rutledge et al. (2004) showed, analyzing microearthquake data detected during hydraulic fracture treatments in the Carthage Cotton Valley, East Texas, gas field, narrow bands of seismicity oriented parallel to the maximum horizontal principal stress direction. These bands correspond to the reservoir's prevalent natural fractures and were shown to correlate with a zone of high-volume flow indicated in another independent observation (Rutledge and Phillips 2003). In fact, many recent studies indicate that fluid-induced earthquakes tend to cluster along preexisting local faults near the fluid injection point that are in accordance with the current stress field (e.g., Kwiatek et al. 2014).

Terakawa et al. (2012) estimated pore fluid pressure field associated with earthquakes induced by fluid injection at Basel, Switzerland. They assumed that variations of focal mechanisms can be attributed to fault strength heterogeneity controlled by variations in pore fluid pressures. Their estimate was based on Coulomb's law of friction with constant static friction coefficient and focal mechanism solutions of induced earthquakes. The estimated pore fluid pressures were approximately consistent with the known history of the wellhead pressure applied at the borehole. In addition, elevated pore fluid pressures were concentrated within 500 m from the injection point, which is consistent with the spatiotemporal evolution of the induced seismicity. This points out that the high-pressure fluid can actually induce earthquake occurrence.

In the water injection experiments at the Nojima fault (Tadokoro et al. 2000) and Matsushiro (Ohtake 1974), it took 4–5 days and nine days to induce seismicity, respectively, after the start of injection as mentioned above. Seismicity began about 10 days after the fluid injection at the Rocky Mountain Arsenal (Healy et al. 1968). We also have an example of the onset of induced events 17 years after the start of injection (Keranen et al. 2013); a similarly long delay was observed at the Cogdell oil field, Texas (Davis and Pennington 1989). Such difference in the time lags may be related to differences in the structure of permeability, pore fluid pressure distribution before the injection, and the pressure and amount of injected fluids in addition to the magnitude of shear and normal stresses acting on faults near the injection well. For example, it is generally known that the permeability is higher a few orders of magnitude in a direction parallel to the fault plane than perpendicular to it (Faulkner and Rutter 2001). Hence, if injection well lies close to well-defined faults as in the studies of Ohtake (1974) and Tadokoro et al. (2000), fluid may flow predominantly along the fault and can induce earthquakes earlier. As another possibility about the cause of the difference in the time lags, we can mention difference in properties of aseismic slip if it occurs prior to the onset of seismicity. In fact, some geodetic data analyses indicate that aseismic slip is induced by the injection of high-pressure fluid (Scotti and Cornet 1994; Bourouis and Bernard 2007; Guglielmi et al. 2015; Wei et al. 2015). Such aseismic slip may be closely related to velocity-strengthening friction properties of fault interface (Bourouis and Bernard 2007), sustained fluid outflow from localized fluid source in an under-stressed medium or slip-induced dilatancy coupled with fluid flow as will be detailed in Sects. 6.2.3 and 6.2.4.

Microearthquake activity induced by fluid injections is commonly interpreted to have resulted from shear failure along preexisting fractures. This is deduced from observations that such events occur all along fractures and that their seismic signals are generally dominated by shear waves. However, fluid injections sometimes trigger nondouble-couple ruptures, which may be an evidence of the involvement of high-pressure fluid. Šílený et al. (2009) actually found predominantly nondouble-couple sources with positive volumetric component by investigating seismicity induced by hydraulic fracturing at the Carthage Cotton Valley, East Texas, gas field. This indicates that crack opening is induced, at least in some cases, by the injection of high-pressure fluid. The existence of volumetric seismic sources has

also been reported at volcanic and geothermal areas (e.g., Dreger et al. 2000; Taira et al. 2010; Shelly et al. 2013b).

It was shown that some active fluid injection areas that have induced earthquakes are susceptible to earthquake triggering from natural transient stresses generated by seismic waves of large remote earthquakes (van der Elst et al. 2013). van der Elst et al. (2013) interpreted this phenomenon as the presence of critically loaded faults and potentially high pore fluid pressure. They also showed that remote triggering of earthquakes occurred with a small delay with respect to the passage of seismic waves, initiating within less than 24 h. They suggested that this pattern of triggered seismicity is closely associated with dynamic permeability enhancement and flow of fluid (e.g., Brodsky et al. 2003).

2.6 Seismicity Induced by the Groundwater Extraction

As stated above, there are a large number of examples suggesting seismicity induced by high-pressure fluid injection. However, examples are also reported that suggest seismicity induced by groundwater extraction (Segall 1989; González et al. 2012). This may occur because the quantity $\sigma_s^0 + \sigma_s + \mu_{stat}(\sigma_n^0 + \sigma_n + p_f^0 + p_f)$, which is generally referred to as Coulomb failure stress, can increase even if groundwater pressure, $p_f^0 + p_f$, decreases near the site of groundwater extraction. Here, σ_s denotes a change of the shear stress acting on the fault from some reference state prior to the slip onset and the superscript 0 denotes the reference state; see Sect. 2.1 about the definition of the other quantities. Fault begins to slip if the condition $\sigma_s^0 + \sigma_s \geq \tau_s$ is satisfied on the fault according to Coulomb's law of friction, where τ_s is the shear strength of fault given by (2.3) with $\mu = \mu_{stat}$. Hence, the Coulomb failure stress represents proximity to slip initiation. Fault begins to slip if the Coulomb failure stress is equal to or greater than zero if the cohesion is negligible as assumed in this chapter, and Chaps. 4–6. González et al. (2012) found that the area of fault slip associated with the 2011 M_w5.1 Lorca, Spain, earthquake that occurred at very shallow depths of 2–4 km correlates well with the pattern of positive change of the Coulomb failure stress caused by the groundwater extraction in a nearby basin aquifer. On the basis of this finding, they interpreted it as meaning that the slip of the 2011 Lorca earthquake was controlled by crustal unloading stress induced by the groundwater extraction.

2.7 Relevance of Slow Earthquakes to the Presence of High-Pressure Fluid

It has become clear in the last decade that there exist a variety of unusual earthquakes that radiate little elastic wave energy. As examples, we can mention tectonic (nonvolcanic) tremor (Obara 2002), slow slip event (SSE) (e.g., Hirose and Obara

2005), low frequency earthquake (LFE) (e.g., Shelly et al. 2006), and very low frequency earthquake (VLFE) (Obara and Ito 2005). Swarm activity of LFEs is regarded as tectonic tremor, which often, but apparently not always, accompanies SSEs (e.g., Obara 2002; Rogers and Dragert 2003). Tectonic tremor, SSE, LFE, and VLFE can collectively be referred to as slow earthquakes because slip evolutions for these events are much slower than those for ordinary earthquakes (Ide et al. 2007).

Recent high-resolution tomography studies (e.g., Shelly et al. 2006) have revealed a zone of high V_p/V_s values in the immediate vicinity of hypocenters of LFEs at subduction zones, which suggests the existence of high-pressure pore fluid and its effect on the generation of LFEs. Wang et al. (2006) and Matsubara et al. (2009) showed that tectonic tremors observed beneath SW Japan are located within a high V_p/V_s zone. Audet and Bürgmann (2014) found by compiling observations in the forearc of circum-Pacific subduction zones that low-velocity zones associated with slow earthquake areas commonly have very high V_p/V_s values. Kato et al. (2010b) found that the distribution of fluid pressure correlates well with the slip rate of long-term slow slip event in the Tokai area, central Japan. Slow migration of tectonic tremors also suggests the involvement of fluid flow (Ito et al. 2007). Remote triggering of LFEs (Miyazawa and Mori 2005) provides indirect evidence for the involvement of high-pressure pore fluid. It may, therefore, be reasonable to consider the effect of fluid flow in understanding the generation mechanism of slow earthquakes. Tanaka et al. (2010) actually found, by measuring spatiotemporal change of gravity, that the occurrence of long-term slow slip event in the Tokai area, Japan, was coupled with fluid flow along the plate interface. It is remarkable that the occurrence of SSEs coupled with tectonic tremors seems to be closely related to the existence of high-pressure pore fluid and its flow according to some theoretical analyses (e.g., Yamashita 2013).

2.8 Relevance of Earthquake Swarm to the Presence of High-Pressure Fluid

2.8.1 Correlation Between the Occurrence of Earthquake Swarm and the Existence of High-Pressure Fluid

Earthquake swarm is a sequence of earthquakes that is not characterized by a dominant event, and the temporal evolution of its activity is not described by any simple law. A clear triggering mechanism, such as magma intrusion, has been identified for earthquake swarms occurring in volcanic areas, but in most cases, their triggering and driving mechanisms are not constrained well. However, usual occurrence of earthquake swarms in volcanic areas, geothermal fields, and ocean ridges (e.g., Fischer et al. 2014) suggests that the occurrence of earthquake swarm is in some way related to the existence of high-pressure fluid. It is now becoming clear

that fluids are very often involved in the generation of earthquake swarms in both intraplate regions and plate margins, too (Kurz et al. 2004). For example, intraplate earthquake swarms without active volcanism occur in continental rifts such as Rio Grande, Kenya, and Western Bohemia (Ibs-von Seht et al. 2008). In these places, the occurrence of earthquake swarms is restricted to deep-reaching zones of weakness that allow intrusion of upper mantle material into crustal layers (Fischer et al. 2014). We also know that injection of high-pressure fluid triggers swarm-like activity as stated above in Sect. 2.5. Hence, it is likely that earthquake swarms have a causal connection with the presence of high-pressure pore fluid and its flow. There also exist some indirect evidences to support this view: (1) slow hypocenter migration (e.g., Hagiwara and Iwata 1968; Hainzl and Fischer 2002; Shelly et al. 2013a), which suggests the involvement of fluid flow, (2) outflow of groundwater simultaneously with the occurrence of earthquake swarm (e.g., Okusawa and Tsukahara 2001; Cappa et al. 2009), (3) correlation of swarm activity with isotopic content of gasses emanating in the source region of swarm (Bräuer et al. 2003; Cappa et al. 2009), (4) triggering of seismic activity in swarm-prone areas from transient stresses generated by the seismic waves of large remote earthquakes (e.g., Yukutake et al. 2011a), for which some different mechanisms are proposed (Hill and Prejean 2015) such as increase in fault-zone permeability (Elkhoury et al. 2011), (5) observation of tensile components of fault slip during swarm activity (Horálek et al. 2002), which suggests opening of slip plane due to fluid pressure elevation, and (5) parabolic spatiotemporal migration patterns quite commonly observed for the migration of earthquake swarm hypocenters (e.g., Shapiro et al. 1997; Hainzl and Ogata 2005; Parotidis et al. 2005; Shelly et al. 2013a); note that parabolic spatiotemporal migration is the solution for a homogeneous and isotropic linear diffusion equation (see Sect. 2.10).

2.8.2 *Driving of Earthquake Swarm by Flow of High-Pressure Fluid and Elastic Stress Transfer*

According to the consideration in Sect. 2.8.1, earthquake swarms seem to have a strong causal relationship with the pressurization of pore fluid and its flow. If this is the case, the fluid is expected to flow predominantly within a fault damage zone, which is, in general, highly permeable in comparison to the surrounding areas (e.g., Lockner et al. 2000); see also Sect. 3.3.1. Recent high-resolution seismological observation clearly shows that earthquake swarms are concentrated on thin planar zones (Yukutake et al. 2011b), which may correspond to preexisting fault segments. Yukutake et al. (2011b) determined the hypocenters and focal mechanisms of earthquake swarm occurred in the caldera of Hakone volcano, central Japan, using data from a dense seismic network. The swarm hypocenters were found to be concentrated on planar zones of thickness about 100 m (Fig. 2.3); in addition, one of the nodal planes of the focal mechanisms agrees with the

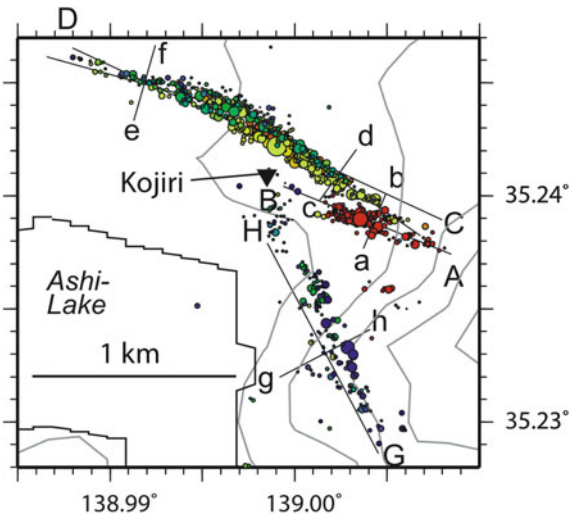

Fig. 2.3 Epicenter distribution of the 2009 Hakone, Japan, earthquake swarm. Depth distributions of hypocenters along cross sections *a–b*, *c–d*, and others are depicted in Yukutake et al. (2011b), which also indicate planar distributions of hypocenters. Yukutake et al. (2011b), reprinted with the permission from John Wiley and Sons

orientation of planar hypocentral distribution. They also observed slow migration of hypocenters of swarm at an initial stage of the activity, which appears to be approximated by a classical linear diffusion equation. The observation of Yukutake et al. (2011b) implies that the earthquake swarm occurred at the Hakone volcano was closely related to the flow of high-pressure fluid within the damage zone at least at an initial stage of its activity. Here, we should note that the occurrence of fault slip also influences the fluid-flow pattern because shear slip generally increases pore space (Yamashita 1999; Suzuki and Yamashita 2014) and permeability (Yeo et al. 1998; Evans et al. 2005) in fault zones. Evans et al. (2005) particularly showed by analyzing fluid injection experiment data that shear slip is the primary mechanism of permeability increase.

Earthquake swarms are not necessarily driven only by the direct effect of high-pressure pore fluid; here, the direct effect means the reduction of effective normal stress by the fluid pressure buildup. Even if swarm activity is driven by the direct effect of high-pressure fluid at an initial stage of activity, evolving slip will redistribute elastic stress. At a later stage of activity, such stress enhancement due to slip accumulation may come into play in driving swarm activity. Yukutake et al. (2011b) actually interpreted a burst-like swarm activity, observed at a later stage of sequence of swarm, as being caused by local elastic stress change by the preceding slips. Hainzl and Fischer (2002) also arrived at the same conclusion, by examining the 2000 Western Bohemia, central Europe, swarm, that the swarm evolution became strongly influenced by the earthquakes themselves due to their stress transfers, while an intrusion of fluid in the seismogenic zone initiated the swarm activity. Catalli et al. (2013) found that the elastic stress transfer plays a more dominant role with time and distance from the injection by analyzing earthquakes induced during the hydraulic stimulation of enhanced geothermal system in Basel, Switzerland. The example studied by Toda et al. (2002) also suggests that stress

transfer played a most dominant role during a sequence of earthquake swarm accompanied by eruptions of the Miyake-jima volcano, Japan. They found that the seismicity rate is proportional to the calculated stressing rate imparted by the dike intrusion.

2.8.3 *Aseismic Slip Coupled with Earthquake Swarm Activity*

The studies mentioned in Sect. 2.8.2 seem to suggest that elastic stress transfer due to slip accumulation plays a dominant role in driving earthquake swarm at a later stage of its activity. However, an emphasis tends to be put on aseismic slip process, in recent studies, in understanding the driving mechanism of earthquake swarm. In fact, aseismically evolving fault slip is found to be coupled with earthquake swarm evolution, at least, in some examples (e.g., Vidale et al. 2006; Lohman and McGuire 2007; Takada and Furuya 2010; Wicks et al. 2011). For example, Wicks et al. (2011) showed, studying earthquake swarm in the Columbia Basin, that the geodetic moment of the modeled fault system is about eight times the cumulative seismic moment of the earthquake swarm. Lohman and McGuire (2007) showed, studying earthquake swarms in the Salton Trough near the southern San Andreas fault system, which is characterized as a transform plate boundary, that recorded seismicity can only explain 20% of the geodetically observed deformation. They interpreted in a way that aseismic fault slip was the primary process driving the swarms in the Salton Trough. Aseismic slip coupled with earthquake swarm is suggested to extend to other regions around the world (e.g., Vidale et al. 2006; Lohman and McGuire 2007; Takada and Furuya 2010; Wicks et al. 2011; Himematsu and Furuya 2015). For example, Takada and Furuya (2010) found on the basis of InSAR and seismological observations that an earthquake swarm occurred in a volcanic area in northeastern Japan (1996 Onikobe, Japan, earthquake swarm) was associated with aseismic slip on reverse faults. Himematsu and Furuya (2015) showed that the 2007 northern Tanzania earthquake swarm that is apparently induced by dike intrusion is also accompanied by relatively large amount of aseismic slip.

While natural earthquakes were investigated in the studies mentioned above, Bourouis and Bernard (2007) showed in the study of seismicity induced during a hydraulic stimulation experiment that swarm activity was forced by aseismic slip resulting from the elevation of fluid pressure. Wei et al. (2015) also showed, analyzing geodetic and seismic wave data, that earthquake swarm was preceded by aseismic slip induced by the injection of high-pressure fluid. Such aseismic slip may be a key for understanding why supposedly induced earthquakes often appear to be substantially offset in time and space with respect to the location and timing of fluid pumping (Wei et al. 2015); see also Sect. 2.5. Guglielmi et al. (2015) directly

observed aseismic slip, monitoring fault movement at the injection zone of high-pressure water, although the injection depth of water (282 m) is much shallower than focal depths of many other earthquake swarms. It is also not clear from the observation at the injection zone alone how the aseismic slip zone expands with fluid pressure change and how the aseismic slip causes seismic activity. The studies of Bourouis and Bernard (2007), Wei et al. (2015), and Guglielmi et al. (2015) anyway suggest that the generation of aseismic slip, which is coupled with natural earthquake swarm, is closely related to the existence of high-pressure fluid. It is noteworthy from such viewpoint that natural earthquake swarms that were found to be coupled with aseismic slip by Lohman and McGuire (2007) lie in an area where hydrothermal activity is relatively high.

We may gain some insight into the generation mechanism of earthquake swarm that is coupled with aseismic slip from observations of tectonic tremors because tectonic tremors have features apparently similar to earthquake swarms. As stated in Sect. 2.7, we can mention as examples of such features: (1) swarm-like activity of tectonic tremors, and (2) occurrence of tectonic tremors concurrently with SSE. This similarity may suggest that tectonic tremors coupled with SSE and earthquake swarm coupled with aseismic slip share a common driving mechanism, although a majority of tectonic tremors occur at depths much deeper than ordinary earthquake swarms. Moreover, it also deserves attention that both SSEs and tectonic tremors seem to be closely related to the existence of high-pressure fluid and its flow (e.g., Yamashita 2013; Shelly 2015); see Sect. 2.7.

The above considerations indicate that aseismic slip and fluid flow will be causally related. In fact, as will be shown theoretically in Chaps. 5 and 6, fluid flow into the slip zone induced by the slip-induced dilatancy can generate sustained aseismic slip evolution if the strength of dilatancy is large enough. Slip-induced porosity generally increases with slip evolution, which tends to inhibit the slip evolution because of the reduction in the effective normal stress. However, the fluid flow into the slip zone induced by the dilatancy gradually weakens the effect of dilatancy and facilitates the slip evolution. A suitable balance between the effects of dilatancy and fluid inflow on the change of effective normal stress gives rise to sustained aseismic slip evolution.

Finally, it may be necessarily to take note of the existence of examples that ground deformation geodetically observed during earthquake swarm does not necessarily require a significant amount of aseismic slip. For example, Holtkamp et al. (2011) geodetically estimated moment release for two earthquake swarms occurred in South America, and found that it is almost the same as the total moment release associated with swarm activity (Holtkamp et al. 2011). This may suggest that the ratio of moment release associated with swarm activity to that due to aseismic slip depends on hydromechanical properties of fault zone or tectonic settings; see Sect. 6.2.5 about the modeling of earthquake swarm accompanied by negligible aseismic slip under the presence of high fluid pressure.

2.9 Contribution of High-Pressure Fluid to Postseismic Deformation of Large Shallow Earthquakes

Large shallow earthquakes are commonly followed not only by aftershocks but also by episodes of slow transients. Such transients are generally attributed to (1) aseismic afterslip, (2) viscoelastic relaxation of ductile lower crust and upper mantle driven by stresses induced by the mainshock, or (3) postseismic rebound of fluid-saturated crust due to pore fluid flow in response to mainshock-induced deformation. Aseismic afterslip is widely observed for shallow large events around the coseismic slip zone (e.g., Ozawa et al. 2004; Perfettini and Avouac 2004); see an example shown in Fig. 2.4. Fluid flow is driven from an undrained state toward a drained state in a process generally referred to as poroelastic rebound; undrained state is defined as a state for which there is no fluid flow, whereas drained state is defined as a state attained after fluid re-equilibrates (see Sect. 4.4). Such fluid flow from an undrained state toward a drained state may play a part in the postseismic deformation. As will be shown in Chap. 4, these two states can be described using the same values of rigidity with a variation in Poisson's ratio; the drained Poisson's ratio is generally smaller than the undrained one: See Sect. 4.6. Consequently, the drained state can be modeled using the coseismic calculation with a reduced Poisson's ratio for the surrounding crust, with the rebound displacements found by taking the difference in predicted surface deformation between the drained and undrained models (e.g., Peltzer et al. 1998; Jónsson et al. 2003; Freed 2007). It should, however, be noted that the process of poroelastic rebound from the undrained to drained state is highly dependent on the fluid-flow pattern as well as the

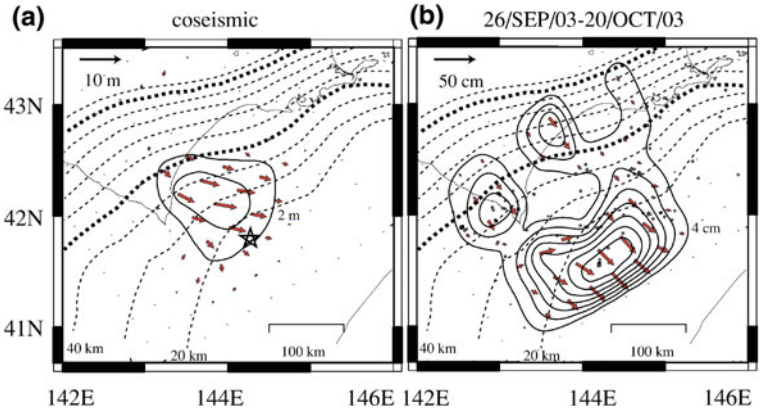

Fig. 2.4 Distributions of **a** coseismic slip and **b** afterslip for the 2003 M_w8.0 Tokachi-Oki, Japan, earthquake. The star in (**a**) denotes the epicenter of the mainshock. Contour intervals for the slip distributions in (**a**) and (**b**) are 2 and 4 m, respectively. *Broken curves* represent iso-depth contours of the plate boundary with 10 km intervals. The *arrows* denote the slip vector. The afterslip is distributed in a way to surround the coseismic slip. Ozawa et al. (2004), reprinted with the permission from Springer

deformation of the medium. Permeability anisotropy, which is generally observed near earthquake faults, may strongly affect the fluid-flow pattern (Sect. 2.5).

Jónsson et al. (2003) studied two magnitude-6.5 earthquakes in south Iceland to identify a dominant mechanism for the postseismic deformation. They found that the deformation recorded in satellite radar interferrograms cannot be explained by either afterslip or viscoelastic deformation, but is consistent with rebound of poroelastic material in the first 1–2 months following the earthquakes. In other words, the observed pattern of LOS (line of sight between the ground and the satellite) displacement is consistent only with the pattern expected from the model of poroelastic rebound. Fialko (2004) studied, analyzing InSAR and GPS data, postseismic deformation due to the 1992 M_w7.3 Landers, California, earthquake. His analysis ruled out afterslip as the only mechanism of postseismic deformation because observed polarity of LOS displacement is opposite to that expected from afterslip. He showed that a combination of poroelastic rebound and afterslip on and below the Landers rupture can explain both InSAR and GPS data about the postseismic deformation. Peltzer et al. (1998) also suggested that a combination of poroelastic rebound and afterslip may explain the pattern of the LOS displacements for the postseismic deformation due to the 1992 Landers earthquake. In contrast to the above studies, Freed (2007) showed, comparing GPS data with finite element modeling, that afterslip is the only mechanism significantly contributing to postseismic deformation following the 2004 M_w6.0 Parkfield, California, earthquake. In fact, postseismic surface deformation expected from poroelastic rebound was found to be significantly smaller than that observed. Gonzalez-Ortega et al. (2014) showed that postseismic deformation of the 2010 M_w7.2 El Mayor-Cucapah, Baja California, earthquake can be explained by a combination of afterslip, fault-zone contraction, and a possible minor contribution of poroelastic rebound.

The studies mentioned above suggest that some underlying mechanisms may be coupled for the generation of postseismic deformation. What is actually observed may be dependent on which mechanism is most dominant in the above coupling; the dominant mechanism may vary with tectonic settings. It may be worthy of note that poroelastic rebound and aseismic afterslip should be coupled each other if we assume slip in a poroelastic medium permeated with fluid. In fact, a possibility was suggested in Sect. 2.8.3 that aseismic slip and fluid flow are causally related. The above consideration indicates that the existence of high-pressure fluid may be a key for understanding apparently diverse postseismic activity.

2.10 Seismological Estimate of Fault-Zone Diffusivity and Permeability

Earthquakes triggered by the injection of high-pressure fluids generally show slow hypocenter migration as stated in Sect. 2.5 (Ohtake 1974; Tadokoro et al. 2000). Earthquake swarms show similar migration pattern. It will be quite natural to

suppose that such hypocenter migration is driven by fluid flow or aseismic slip induced by the fluid flow. Assuming fluid flow as a dominant driving mechanism of swarm activity, many researchers tried to estimate fault-zone permeability or hydraulic diffusivity by comparing the migration speed of hypocenters with a solution of linear fluid diffusion equation. We, however, have to note that fault-zone permeability is, in general, a highly fluctuating parameter of rocks strongly influenced by the heterogeneities of pore space; the permeability can vary by orders of magnitude, even for adjacent locations (e.g., Brace 1980).

Many researchers actually assume a linear diffusion equation of type

$$\frac{\partial p_{\mathrm{f}}}{\partial t} = D_{ij} \frac{\partial^2 p_{\mathrm{f}}}{\partial x_i \partial x_{\mathrm{f}}} \tag{2.4}$$

in the estimate of hydraulic diffusivity or permeability, where p_{f} is the fluid pressure change, D_{ij} is the ij component of hydraulic diffusivity tensor, t is time, and x_i is one of the spatial coordinates. However, we have to note, as will be shown in Sect. 4.7, that (2.4) is valid only in an extreme case when the fluid pressure change does not couple with the volumetric change of poroelastic medium and D_{ij} is homogeneous over the medium. The hydraulic diffusivity tensor D_{ij} is proportional to the permeability tensor K_{ij} in a form

$$D_{ij} = \frac{MK_{ij}}{\eta} \tag{2.5}$$

if the form of (4.53) is assumed, where η is the fluid viscosity and M is a parameter referred to as the Biot modulus (see Table 4.1). Once the values of M and η are given, we can obtain the value of permeability from the estimate of hydraulic diffusivity. Although a number of researchers assumed constant and isotropic diffusivities in the estimate of hydraulic diffusivity, Antonioli et al. (2005) took account of anisotropy in the hydraulic diffusivity and Miller et al. (2004) assumed that the scalar hydraulic diffusivity is dependent on the effective normal stress.

Shapiro et al. (1997) proposed a relation

$$r = \sqrt{4\pi D t}, \tag{2.6}$$

taking account of a solution for a linear spherically symmetrical diffusion equation, where D is scalar isotropic hydraulic diffusivity, r is the distance of triggering front of seismicity measured from the injection point of fluid (or source of high-pressure fluid), and t is time. In the derivation of (2.6), Shapiro et al. (1997) assumed a diffusion equation

$$\frac{\partial p_{\mathrm{f}}}{\partial t} = D\nabla^2 p_{\mathrm{f}} = \frac{D}{r^2}\frac{\partial}{\partial r}\left(r^2 \frac{\partial p_{\mathrm{f}}}{\partial r}\right) \tag{2.7}$$

in the presence of spherical symmetry to examine the fluid pressure change in the region $r > a$ that is caused by a time-harmonic fluid pressure perturbation $p_f(t) = p_0 \exp(-i\omega t)$ applied at the boundary $r = a$, where ω is the angular frequency and the location $r = 0$ is regarded as the fluid injection point. They obtained a solution in a form

$$p_f(t) = p_0 \frac{a}{r} \exp(-i\omega t) \exp\left[(i-1)(r-a)\sqrt{\frac{\omega}{2D}}\right], \tag{2.8}$$

which represents an exponentially decaying spherical wave. Equation (2.8) suggests that the propagation velocity of fluid pressure disturbance is given by $\sqrt{2D\omega}$. They assumed that triggering of a seismic event at time t_0 is due to a rectangular pulse $p_f(t) = p_c[H(t) - H(t - t_0)]$ applied at $r = a$ since the evolution of injection for $t > t_0$ is irrelevant to this event, where $H(\cdot)$ is a unit step function. If such rectangular pulse is assumed, the dominant frequencies of this signal are in a range from 0 to $\omega_0 = 2\pi/t_0$. Thus, if even a slight increase in the fluid pressure triggers seismicity, the propagation velocity of triggering front will be given by $\sqrt{4D\pi/t_0}$, which yields (2.6). Equation (2.6) may be an order-of-magnitude estimate as suggested by the above analysis.

Shapiro et al. (1997) estimated hydraulic diffusivity comparing (2.6) with spatiotemporal distribution of injection-induced earthquakes at the KTB deep drilling site, Germany. Subsequently, many researchers estimated values of hydraulic diffusivity assuming (2.6) for earthquake swarms and events triggered by the injection of high-pressure fluid probably because of its simplicity; estimated values for earthquake swarms are found to be in a range $0.1-1.5\,\mathrm{m}^2/\mathrm{s}$ as exemplified in Fig. 2.5 and Table 2.1. Chen et al. (2012) found that the value $\sim 1.0\,\mathrm{m}^2/\mathrm{s}$ is roughly the upper end of estimates except limited examples.

The approach based on (2.6) is generally regarded as being valid if (1) the state of stress in the crust is very close to a critical one, (2) hydraulic diffusivity of crustal rocks is isotropic and constant, (3) the pore-pressure field is decoupled from seismic rupturing and related stress changes, and (4) stress enhancement due to evolving slip is much smaller than the fluid pressure elevation due to its flow; see Fischer et al. (2014). However, if the condition (1) is satisfied over a large area, the growth of triggered ruptures will be accelerated with time and grow indefinitely. This problem may be circumvented if we introduce an additional condition (5) that suppresses such indefinite rupture propagation. We have to note that the conditions (1)–(4) will not necessarily be satisfied in all earthquake swarms. For example, there exists a possibility of coupling between permeability change and fault slip evolution (Sects. 4.10 and 6.1); see also Miller (2015) and references therein. In addition, fluid may flow predominantly along preexisting fault zones because of the existence of high-permeability damage zone juxtaposed with the fault core; the fault core, which will have low permeability in interseismic periods, may turn to high permeable one with the onset of slip because of the creation of slip-induced pores. Seismological observations showing the concentration of swarm earthquakes on

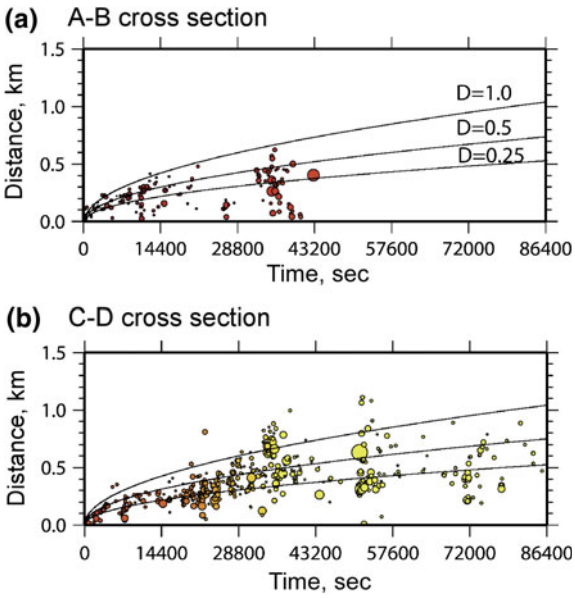

Fig. 2.5 Spatiotemporal distribution of hypocenters of the 2009 Hakone, Japan, earthquake swarm along cross sections **a** *A–B* and **b** *C–D* illustrated in Fig. 2.3. The origin of the coordinates is assumed at the location of the first event in each sequence of activity. Three different values are assumed for the hydraulic diffusivity $D(\text{in m}^2/\text{s})$ to fit to the distribution of hypocenters. We observe that the migration velocity of seismicity is on the order of m/h. Burst-like seismic activities may be related to elastic stress transfer (Yukutake et al. 2011b). Yukutake et al. (2011b), reprinted with the permission from John Wiley and Sons

thin planar zones actually suggest fluid flow predominantly along preexisting fault zones (e.g., Yukutake et al. 2011b; Shelly et al. 2013a, b; Hauksson et al. 2016); see also related discussion in Sect. 2.8. As mentioned at the beginning of this section, extreme heterogeneity of hydraulic properties in the upper crust may also significantly affect the fluid flow. Hence, the assumption of constant and isotropic hydraulic diffusivity may be an oversimplification. In addition, sudden onsets of seismicity burst, which may occur because of cascading ruptures, are sometimes observed in the evolution of earthquake swarm (e.g., Yukutake et al. 2011b; Hauksson et al. 2016) as exemplified in Fig. 2.5. This gives rise to sptaio-temporal hypocenter distribution that is much more complex than expected from (2.6). Cascading ruptures will occur because of sudden stress enhancement due to the occurrence of relatively large size event, so that the condition (4) stated above is not necessarily satisfied. However, if the condition (5) is satisfied, infinite cascading will be suppressed. In Chap. 6, we will assume both slip-induced dilatancy and low tectonic stress as a mechanism to suppress the indefinite rupture propagation.

It may be meaningful to remark here that some earthquake swarms that are considered to be driven by aseismic slip have migration velocities much higher than observed in injection-induced earthquakes and earthquake swarms that appear to

Table 2.1 Seismological estimates of hydraulic diffusivity

Events	Estimated hydraulic diffusivity
1983 Hydraulic injection at Fenton Hill, New Mexico	0.17 m^2/s[a]
1989 Mammoth Mountain earthquake swarm, California	0.2–0.8 m^2/s[b]
1994 Hydraulic injection at KTB, Germany	~0.1 m^2/s[c]
2000 and 2008 Western Bohemia earthquake swarms, central Europe	~0.3 m^2/s[d,e]
2001 Agios Ioanis earthquake swarm, Greece	~0.1 m^2/s[f]
2002 Mt. Hochstaufen earthquake swarm, Germany	~0.75 m^2/s[g]
2009 Hakone earthquake swarm, Japan	0.5–1.0 m^2/s[h]
2009 Mount Rainier earthquake swarm, Washington	~1 m^2/s[i]
2010 Madison Plateau earthquake swarm, Yellowstone Caldera	~1.5 m^2/s[j]

[a]Shapiro et al. (2002)
[b]Hill and Prejean (2005)
[c]Shapiro et al. (1997)
[d]Hainzl and Ogata (2005)
[e]Hainzl et al. (2012)
[f]Pacchiani and Lyon-Caen (2010)
[g]Kraft et al. (2006)
[h]Yukutake et al. (2011b)
[i]Shelly et al. (2013a)
[j]Shelly et al. (2013b)

have been driven dominantly by high-pressure fluid flow. In fact, seismicity driven by aseismic slip at strike-slip plate boundary has been observed to migrate at velocities on the order of km/h (Roland and McGuire 2009), whereas the migration of seismicity apparently driven by fluid flow propagates at speeds on the order of m/h as exemplified in Fig. 2.5. Migration velocities on the order of km/h correspond to the rupture propagation velocity of shallow creep transients observed geodetically in conjunction with swarms (Roland and McGuire 2009). However, as will be shown in theoretical analyses in Sect. 6.2, we cannot eliminate a possibility that even aseismic slip on the order of km/h can be caused by the fluid flow.

Although Shapiro et al. (1997) seem to have considered relatively general situation for the fluid pressure source, we can easily derive analytical solutions for the spatiotemporal change of fluid pressure if we assume simple models for the fluid pressure source. We may be able to obtain some insight from such solutions. Let us now assume two specific examples of fluid pressure source $p_f(t) = p^c H(t)$ and $p_f(t) = p^c \delta(t)$ located at $r = a$ in an infinite fluid-saturated poroelastic medium having a property of spherical symmetry, where p^c is a positive constant and $\delta(\cdot)$ is Dirac's delta function. The solutions are written as

$$p_f(t,r) = \frac{ap^c}{r}\left[1 - \mathrm{erf}\left(\frac{(r-a)}{\sqrt{4Dt}}\right)\right] \text{ for the source } p_f(t) = p^c H(t), \tag{2.9}$$

$$p_{\mathrm{f}}(t,r)=\frac{ap^{c}}{r}\frac{r-a}{t\sqrt{4\pi Dt}}\exp\left(-\frac{(r-a)^{2}}{4Dt}\right)\ \text{for the source}\ p_{\mathrm{f}}(t)=p^{c}\delta(t) \tag{2.10}$$

for $t>0$ and $r\geq a$ (see Appendix of this chapter), where $\mathrm{erf}(\cdot)$ is the error function defined by (2.19). We illustrate in Fig. 2.6 the spatiotemporal change of these solutions. Specifically, we show how the terms $1-\mathrm{erf}\left[(r-a)/\sqrt{4Dt}\right]$ in (2.9) and $\left[(r-a)/\sqrt{4Dt}\right]^{3}\exp\left[-(r-a)^{2}/4Dt\right]$ in (2.10) change with the change of $(r-a)/\sqrt{4Dt}$. The fluid pressure change takes a maximum value at $r-a=\sqrt{6Dt}$ for the solution (2.10), so that if the fluid pressure elevation triggers seismicity, it should occur in a time range $r-a\geq\sqrt{6Dt}$. Equation (2.6) proposed as the triggering front by Shapiro et al. (1997) satisfies this condition, although the assumption about the temporal change of fluid pressure source is largely different. Figure 2.6 also shows that (2.6) is satisfied at smooth and gradual onset of fluid pressure change for the solution (2.9). The examples considered here suggest that although the relation (2.6) does not contradict with the expectation from (2.9) and (2.10), there is much uncertainty about the estimate of hydraulic diffusivity even if the fluid flow in a medium with spherical symmetry is appropriate.

Some researchers estimated permeabilities or hydraulic diffusivities without relying on the relation (2.6). For example, Ohtake (1974) estimated values of

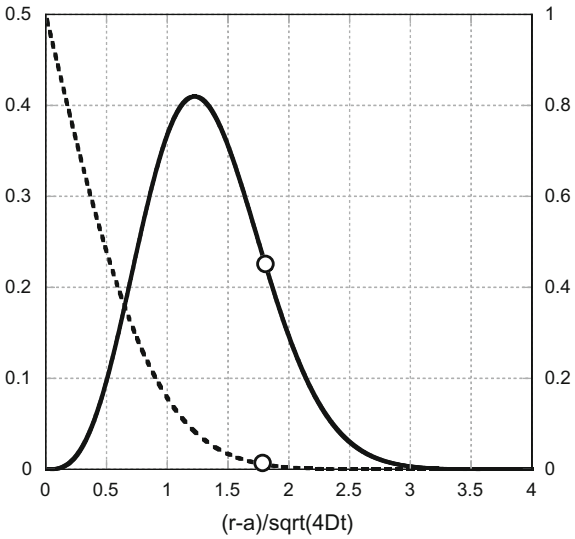

Fig. 2.6 Changes of $1-\mathrm{erf}\left[(r-a)/\sqrt{4Dt}\right]$ (*broken curve*) and $\left[(r-a)/\sqrt{4Dt}\right]^{3}\exp\left[-(r-a)^{2}/4Dt\right]$ (*solid curve*) with $(r-a)/\sqrt{4Dt}$. Refer to the *left* and *right* ordinates about the *solid* and *broken curves*, respectively. The *open circles* shows the location $(r-a)=\sqrt{4\pi Dt}$, which corresponds to (2.6)

fault-zone permeability at Matsushiro, central Japan, assuming that temporal change of fluid pressure should have a peak value between the onset and termination times of seismic activity triggered by the injection of high-pressure water. He compared the spatiotemporal change of seismic activity with that of fluid pressure obtained by solving a 2D linear diffusion equation. He estimated the permeability in a range from 10^{-14} to 10^{-13} m^2 assuming some appropriate values for M and η. Tadokoro et al. (2000) used the same procedure as assumed by Ohtake (1974) and estimated the permeability of rocks constituting the Nojima fault zone to be 10^{-14}–10^{-13} m^2 on the basis of seismicity triggered by the high-pressure water injection into the 1800-m deep well. Miller et al. (2004) obtained the value of fault-zone permeability 4×10^{-11} m^2 for an aftershock sequence occurred in northern Italy in 1997; they considered that the sequence was driven by high-pressure CO_2 source at depth. Their estimate is based on comparison between the observed migration velocity of hypocenters with an analytical solution of 2D nonlinear diffusion equation, in which the permeability was assumed to be a strongly decreasing function of the effective normal stress. Wave-like solution is obtained for such pressure-dependent permeability, in contrast to a more diffuse front resulting from a linear diffusion equation such as (2.7). Antonioli et al. (2005) also analyzed the aftershock sequence studied by Miller et al. (2004). A difference between the two studies is that Antonioli et al. (2005) assumed anisotropic permeability, while Miller et al. (2004) did isotropic one. The permeability component was found to be largest in the strike direction of major faults, which is 7.4×10^{-12} m^2. This suggests that high-pressure fluid tends to migrate along preexisting faults, which is consistent with the seismological observations of Yukutake et al. (2011b) and Shelly et al. (2013a, b). Nippress and Rietbrock (2007) analyzed aftershock sequence of the 1995 M_w8.0 Antofagasta, Northern Chile, earthquake. They interpreted a seismicity streak extending from the seismogenic zone into the overlying continental crust as ruptures driven by upward fluid migration through a preexisting fracture zone. They estimated continental crust permeability to be 10^{-14} to 10^{-15} m^2 by comparing the evolution speed of seismic activity with the characteristic time for the diffusion $t = r^2/D$ [see (2.6), (2.9) and (2.10)]. Hainzl et al. (2006) found, using high-resolution data, that rainfall triggered swarm-like earthquake activity below Mt. Hochstaufen, SE Germany. They investigated the effect of rainfall on seismicity, assuming a 1D linear diffusion equation; the concept of rate and state dependence of frictional strength was assumed to simulate seismicity rate. They found a hydraulic diffusivity 3.3 m^2/s, which corresponds well to the range of values tabulated in Table 2.1. The triggering of seismicity by rainfall suggests that the crust is on a close-to-failure condition at least at Mt. Hochstaufen. Although values of permeability and hydraulic diffusivity were estimated by many authors as exemplified above, theoretical models on which their estimates are based are diverse and the appropriateness of models to individual phenomena is not very clear. It may be required to study how the difference in the assumption of theoretical model affects the estimate of permeability or hydraulic diffusivity.

There are examples of laboratory measurements of fault-zone permeabilities. These measurements have shown that the fault core has generally much lower permeability than that measured in the surrounding damage zone. Comparison between such laboratory measurements and estimates based on migration of seismicity may be helpful to understand the appropriateness of the seismological estimate of fault-zone permeability. For example, Lockner et al. (2000) measured permeability of core samples taken from two drill holes that crossed the Nojima fault at depths 624 and 1140 m that slipped at the time of 1995 M_w6.9 Hyogo-ken Nanbu (Kobe), Japan, earthquake. They found that the permeabilities at the fault core and damage zone are about 10^{-18} and 10^{-16} m^2, respectively, at depth 1140 m. Mizoguchi et al. (2008) also studied the Nojima fault-zone permeability and found that it consists of a low-permeability fault gouge zone on the order of 10^{-20}–10^{-19} m^2 within a high-permeability damaged zone of fault breccia and fractured host rock on the order of 10^{-18}–10^{-14} m^2. As mentioned above, the estimate by Tadokoro et al. (2000) based on the migration of seismicity was 10^{-14}–10^{-13} m^2, which are much larger than the estimates by Lockner et al. (2000) and Mizoguchi et al. (2008). This difference may partly be because dynamic slips associated with the seismic activity observed by Tadokoro et al. (2000) create new fractures and pores during their evolution on and around the fault (e.g., Segall and Rice 1995; Yamashita 1999; Suzuki and Yamashita 2010), which enhances the permeability. It is, however, difficult to estimate the value of fault-zone permeability taken during dynamic slip evolution using core samples collected somewhat after the slip occurrence: Fault-zone permeability tends to decrease with time because of fault healing (Kitagawa et al. 2007).

Appendix: Analytical Solutions for Spherically Symmetric Diffusion Equation

We first solve (2.7) under the boundary conditions

$$p_f = p^c H(t) \quad \text{at } r = a, \tag{2.11}$$

$$p_f \to 0 \quad \text{at } r \to +\infty \tag{2.12}$$

and the initial condition

$$p_f = 0 \quad \text{for } a \le r < +\infty, \tag{2.13}$$

where $H(t)$ is a unit step function. If we assume a relation $q = rp_f$, (2.7) is reduced to

$$\frac{\partial q}{\partial t} = D\frac{\partial^2 q}{\partial r^2}, \tag{2.14}$$

which is now solved by the Laplace transform in time t

$$q^*(r,s) = \int_0^\infty q(r,t)\exp(-st)\mathrm{d}t. \tag{2.15}$$

The solution is then given in a form

$$q^*(r,s) = a_0(s)\exp(-r\sqrt{s/D}) \tag{2.16}$$

if (2.12) and (2.13) are taken into account. The parameter $a_0(s)$ is determined by (2.11). We then have

$$q^*(r,s) = \frac{ap^c}{s}\exp\left[-(r-a)\sqrt{s/D}\right]. \tag{2.17}$$

By carrying out the inverse Laplace transform and taking account of the relation $q = rp_\mathrm{f}$, we have the solution

$$p_\mathrm{f}(t,r) = \frac{ap^c}{r}\left[1 - \mathrm{erf}\left(\frac{(r-a)}{\sqrt{4Dt}}\right)\right] \quad \text{for } t > 0, \tag{2.18}$$

where $\mathrm{erf}(\cdot)$ is the error function defined as

$$\mathrm{erf}(x) = \frac{2}{\sqrt{\pi}}\int_0^x \exp(-s^2)\mathrm{d}s. \tag{2.19}$$

See Sect. 4.15.3 as to the inverse Laplace transform. The solution corresponding to the boundary condition $p_f(t) = p^c\delta(t)$ at $r = a$ is given by differentiating the right-hand side of (2.18) with respect to t in a form

$$p_\mathrm{f}(t,r) = \frac{ap^c}{r}\frac{r-a}{t\sqrt{4\pi Dt}}\exp\left(-\frac{(r-a)^2}{4Dt}\right) \quad \text{for } t > 0. \tag{2.20}$$

References

Antonioli A, Piccinini D, Chiaraluce L, Cocco M (2005) Fluid flow and seismicity pattern: evidence from the 1997 Umbria-Marche (central Italy) seismic sequence. Geophys Res Lett 32:L10311. doi:10.1029/2004GL022256

Audet P, Bürgmann R (2014) Possibile control of subduction zone slow-earthquake periodicity by silica enrichment. Nature 510:389–392. doi:10.1038/nature13391

Bourouis S, Bernard P (2007) Evidence for coupled seismic and aseismic fault slip during water injection in the geothermal site of Soultz (France), and implications for seismogenic transients. Geophys J Int 169:723–732. doi:10.1111/j.1365-246X.2006.03325.x

Brace WF (1972) Pore pressure in geophysics. In: Heard HC, Borg IY, Carter NL, Raleigh CB (eds) Flow and fracture of rocks. Amer Geophys Union, Washington, pp 265–273 (Geophys Monogr 16)

Brace WF (1980) Permeability of crystalline and argillaceous rocks. Int J Rock Mech Min Sci 17:241–251

Bräuer K, Kämpf H, Strauch G, Weise SM (2003) Isotopic evidence ($^3He/^4He$, $^{13}C_{CO2}$) of fluid-triggered intraplate seismicity. J Geophys Res 108:2070. doi:10.1029/2002JB002077

Brodsky EE, Roeloffs E, Woodcock D, Gall I, Manga M (2003) A mechanism for sustained groundwater pressure changes induced by distant earthquakes. J Geophys Res 108:2390. doi:10.1029/2002JB002321

Cappa F, Rutqvist J, Yamamoto K (2009) Modeling crustal deformation and rupture processes related to upwelling of deep CO_2-rich fluids during the 1965–1967 Matsushiro earthquake swarm in Japan. J Geophys Res 114:B10304. doi:10.1029/2009JB006398

Carder DS (1945) Seismic investigations in the Boulder Dam area, 1940-1944, and the influence of reservoir loading on earthquake activity. Bull Seismol Soc Amer 35:175–192

Catalli F, Meier MA, Wiemer S (2013) The role of Coulomb stress changes for injection—induced seismicity: The Basel enhanced geothermal system. Geophys Res Lett 40:72–77. doi:10.1029/2012GL054147

Chen X, Shearer PM, Abercrombie RE (2012) Spatial migration of earthquakes within seismic clusters in Southern California: Evidence for fluid diffusion. J Geophys Res 117:B04301. doi:10.1029/2011JB008973

Christensen NI (1984) Pore pressure and oceanic crustal seismic structure. Geophys J R Astron Soc 79:411–424

Christensen NI (1996) Poisson's ratio and crustal seismology. J Geophys Res 101:3139–3156. doi:10.1029/95JB03446

Dahm T, Fischer T (2013) Velocity ratio variations in the source region of earthquake swarms in NW Bohemia obtained from arrival time double-differences. Geophys J Int 196:957–970. doi:10.1093/gji/ggt410

Davies R, Foulger G, Bindley A, Styles P (2013) Induced seismicity and hydraulic fracturing for the recovery of hydrocarbons. Mar Petrol Geol 45:171–185

Davis SD, Pennington WD (1989) Induced seismic deformation in the Cogdell oil field of west Texas. Bull Seismol Soc Amer 79:1477–1494

Dawson PB, Chouet BA, Okubo PG, Villaseñor A, Benz HM (1999) Three-dimensional velocity structure of the Kilauea caldera, Hawaii. Geophys Res Lett 26:2805–2808

Dreger DS, Tkalčić H, Johnston M (2000) Dilatational processes accompanying earthquakes in the Long Valley caldera. Science 288:122–125. doi:10.1126/science.288.5463.122

Eberhart-Phillips D, Michael AJ (1993) Three dimensional velocity structure, seismicity, and fault structure in the Parkfield region, central California. J Geophys Res 98:15737–15758

Eberhart-Phillips D, Stanley WD, Rodriguez BD, Lutter WJ (1995) Surface seismic and electrical methods to detect fluids related to faulting. J Geophys Res 100:12919–12936

Elkhoury JE, Niemeijer A, Brodsky E, Marone C (2011) Laboratory observations of permeability enhancement by fluid pressure oscillations of an in situ fractured rock. J Geophys Res 116:B02311. doi:10.1029/2010JB0077599

Ellsworth WL (2013) Injection-induced earthquakes. Science 341:1225942. doi:10.1126/science.1225942

Evans DM (1966) Denver area earthquakes and the Rocky Mountain Arsenal disposal well. Mt Geol 3:23–36

Evans KF, Genter A, Sausss J (2005) Permeability creation and damage due to massive fluid injections into granite at 3.5 km at Soultz: 1. Borehole observations. J Geophys Res 110: B04203. doi:10.1029/2004JB003168

Faulkner DR, Rutter EH (2001) Can the maintenance of overpressured fluids in large strike-slip fault zones explain their apparent weakness? Geology 29:503–506

Fialko Y (2004) Evidence of fluid-filled upper crust from observations of postseismic deformation due to the 1992 Mw7.3 Landers earthquake. J Geophys Res 109:B08401. doi:10.1029/2004JB002985

Fischer T, Horálek J, Hrubcová, V. Vavryčuk V, Bräuer K, Kämpf H (2014) Intra-continental earthquake swarms in West-Bohemia and Vogtland: a review. Tectonophysics 611:1–27

Freed AM (2007) Afterslip (and only afterslip) following the 2004 Parkfield, California, earthquake. Geophys Res Lett 34:L06312. doi:10.1029/2006GL029155

Garbin HD, Knopoff L (1975) Elastic moduli of a medium with liquid-filled cracks. Q Appl Math 32:301–303

González PJ, Tiampo KF, Palano M, Cannavó F, Fernández J (2012) The 2011 Lorca earthquake slip distribution controlled by groundwater crustal unloading. Nat Geosci 5:821–825. doi:10.1038/NGEO1610

Gonzalez-Ortega A, Fialko Y, Sandwell D, Nava-Pichardo FA, Fletcher J, Gonzalez-Garcia J, Lipovsky B, Floyd M, Funning G (2014) El Mayor-Cucapah (Mw 7.2) earthquake: early near-field postseismic deformation from InSAR and GPS observations. J Geophys Res 119:1482–1497. doi:10.1002/2013JB010193

Guglielmi Y, Cappa F, Avouac JP, Henry P, Elsworth D (2015) Seismicity triggered by fluid injection-induced aseismic slip. Science 348:1224–1226. doi:10.1126/science.aab0476

Gupta HK (1992) Reservoir-induced earthquakes. Elsevier, Amsterdam

Gupta HK (2002) A review of recent studies of triggered earthquakes by articifial water reservoirs with special emphasis on earthquakes in Koyna, India. Earth Sci Rev 58:279–310

Gupta HK, Rastogi BK (1976) Dams and earthquakes. Elsevier, Amsterdam

Hacker BR, Abers GA (2012) Subduction factory 5: unusually low Poisson's ratios in subduction zones from elastic anisotropy of peridotite. J Geophys Res 117:B06308. doi:10.1029/2012JB009187

Hagiwara T, Iwata T (1968) Summary of the seismographic observation of Matsushiro swarm earthquakes. Bull Earthq Res Inst 46:485–515

Hainzl S, Fischer T (2002) Indications for a successively triggered rupture growth underlying the 2000 earthquake swarm in Vogtland/NW Bohemia. J Geophys Res 107:2338. doi:10.1029/2002JB001865

Hainzl S, Ogata Y (2005) Detecting fluid signals in seismicity data through statistical earthquake modeling. J Geophys Res 110:B05S07. doi:10.1029/2004JB003247

Hainzl S, Kraft T, Wassermann J, Igel H, Schmedes E (2006) Evidence for rainfall-triggered earthquake activity. Geophys Res Lett 33:L19303. doi:10.1029/2006GL027642

Hainzl S, Fischer T, Dahm T (2012) Seismicity-based estimation of the driving fluid pressure in the case of swarm activity in western Bohemia. Geophys J Int 191:271–281

Hauksson E, Andrews J, Plesch A, Shaw JH, Shelly DR (2016) The 2015 Fillmore earthquake swarm and possible crustal deformation mechanisms near the bottom of the eastern Ventura basin, California. Seismol Res Lett 87:807–815

Healy JH, Rubey WW, Griggs DT, Raleigh CB (1968) The Denver earthquake. Science 161:1301–1310

Hill DP, Prejean SG (2005) Magmatic unrest beneath Mammoth Mountain, California. J Volcanol Geotherm Res 146:258–283

Hill DP, Prejean SG (2015) Dynamic triggering. In: Schubert G (ed) Treatise on geophysics, vol 4, 2nd edn. Elsevier, Amsterdam, pp 273–304

Himematsu Y, Furuya M (2015) Aseismic strike–slip associated with the 2007 dike intrusion episode in Tanzania. Tectonophysics 656:52–60

Hirose H, Obara K (2005) Repeating short- and long-term slow slip events with deep tremor activity around the Bungo channel region, southwest Japan. Earth Planets Space 57:961–972

Holtkamp SG, Pritchard ME, Lohman RB (2011) Earthquake swarms in south America. Geophys J Int 187:128–146. doi:10.1111/j.1365-246X.2011.05137.x

Horálek J, Šílený J, Fischer T (2002) Moment tensors of the January 1997 earthquake swarm in NW Bohemia (Czech Republic): double-couple vs. non-double-couple events. Tectonophysics 356:65–85

Hubbert MK, Rubey WW (1959) Role of fluid pressure in mechanics of overthrust faulting, 1. Mechanics of fluid-filled porous solids and its application to overthrust faulting. Bull Geol Soc Amer 70:115–166

Ibs-von Seht M, Plenefisch T, Klinge K (2008) Earthquake swarms in continental rifts—a comparison of selected cases in America, Africa and Europe. Tectonophysics 452:66–77. doi:10.1016/j.tecto.2008.02.008

Ide S, Beroza G, Shelly DR, Uchide T (2007) A scaling law for slow earthquakes. Nature 447: 76–79. doi:10.1038/nature05780

Ito Y, Obara K, Shiomi K, Sekine S, Hirose H (2007) Slow earthquakes coincident with episodic tremors and slow slip events. Science 315:503–506. doi:10.1126/science.1134454

Jónsson S, Segall P, Pedersen R, Björnsson G (2003) Post-earthquake ground movements correlated to pore-pressure transients. Nature 424:179–183. doi:10.1038/nature01776

Kamiya S, Kobayashi Y (2000) Seismological evidence for the existence of serpentinized wedge mantle. Geophys Res Lett 27:819–822

Kato A, Sakai S, Iidaka T, Iwasaki T, Hirata N (2010a) Non-volcanic seismic swarms triggered by circulating fluids and pressure fluctuations above a solidified diorite intrusion. Geophys Res Lett 37:L15302. doi:10.1029/2010GL043887

Kato A, Iidaka T, Ikuta R, Yoshida Y, Katsumata K, Iwasaki T, Sakai S, Thurber C, Tsumura N, Yamaoka K, Watanabe T, Kunitomo T, Yamazaki F, Okubo M, Suzuki S, Hirata N (2010b) Variations of fluid pressure within the subducting oceanic crust and slow earthquakes. Geophys Res Lett 37:L14310. doi:10.1029/2010GL043723

Keranen KM, Savage HM, Abers GA, Cochran ES (2013) Potentially induced earthquakes in Oklahoma, USA: links between wastewater injection and the 2011 Mw 5.7 earthquake sequence. Geology 41:699–702

Kitagawa Y, Fujimori K, Koizumi N (2007) Temporal change in permeability of the Nojima fault zone by repeated water injection experiments. Tectonophysics 443:183–192

Kraft T, Wassermann J, Schmedes E, Igel H (2006) Meteorological triggering of earthquake swarms at Mt. Hochstaufen, SE-Germany. Tectonophysics 424:245–258. doi:10.1016/j.tecto.2006.03.044

Kurashimo E, Hirata N (2004) Low V_P and V_P/V_S zone beneath the northern Fossa Magna basin, central Japan, derived from a dense array observation. Earth Planets Space 56:1301–1308

Kurz JH, Jahr T, Jentzsch G (2004) Earthquake swarm examples and a look at the generation mechanism of the Vogtland/Western Bohemia earthquake swarms. Phys Earth Planet Inter 142:75–88. doi:10.1016/j.pepi.2003.12.007

Kwiatek G, Buluta F, Bohnhoffa M, Dresena G (2014) High-resolution analysis of seismicity induced at Berlín geothermal field, El Salvador. Geothermics 52:98–111. doi:10.1016/j.geothermics.2013.09.008

Lee WHK, Raleigh CB (1969) Fault-plane solution of the Koyna (India) earthquake. Nature 223:172–173

Li YG, Chen P, Cochran ES, Vidale JE, Burdette T (2006) Seismic evidence for rock damage and healing on the San Andreas Fault associated with the 2004 M6.0 Maule earthquake. Bull Seismol Soc Am 96:S349–S363. doi:10.1785/0120050803

Lockner D, Naka H, Tanaka H, Ito H, Ikeda R (2000) Permeability and strength of core samples from the Nojima fault of the 1995 Kobe earthquake. In: Ito H, Fujimoto K, Tanaka H, Lockner F (eds) Proceedings of the internat. Workshpp on the Nojima Fault core and borehole data analysis, Tsukuba, Japan, 22–23 Nov 1999. USGS Open File Report 00-129

Lohman RB, McGuire JJ (2007) Earthquake swarms driven by aseismic creep in the Salton Trough, California. J Geophys Res 112:B04405. doi:10.1029/2006JB004596

Matsubara M, Obara K, Kasahara K (2009) High-V_P/V_S zone accompanying non-volcanic tremors and slow-slip events beneath southwestern Japan. Tectonophysics 472:6–17. doi:10.1016/j.tecto.2008.06.013

Miller SA (2015) Modeling enhanced geothermal systems and the essentialnature of large-scale changes in permeability at the onset of slip. Geofluids 15:338–349. doi:10.1111/gfl.12108

Miller SA, Colletini C, Chiaraluce L, Cocco M, Barchi M, Kaus BJP (2004) Aftershocks driven by a high-pressure CO_2 source at depth. Nature 427:724–727. doi:10.1038/nature02251

Miyazawa M, Mori J (2005) Detection of triggered deep low frequency events from the 2003 Tokachi-oki earthquake. Geophys Res Lett 32:L10307. doi:10.1029/2005GL022539

Mizoguchi K, Hirose T, Shimamoto T, Fukuyama E (2008) Internal structure and permeability of the Nojima fault, southwest Japan. J Struct Geol 30:513–524

Moreno M, Haberland C, Oncken O, Rietbrock A, Angiboust S, Heidbach O (2014) Locking of the Cile subduction zone controlled by fluid pressure before the 2010 earthquake. Nat Geosci 7:292–296. doi:10.1038/NGEO2102

Morrow C, Radney B, Byerlee J (2002) Frictional strength and effective pressure law of montmorillonite and illite clays. In: Evans B, Wong TF (eds) Fault mechanics and transport properties of rocks. Academic Press, New York, pp 69–88

Nakajima J, Matsuzawa T, Hasegawa A, Zhao D (2001) Three-dimensionasl tructure of Vp, Vs, and Vp/Vs beneath northeastern Japan: implications for arc magmatism and fluids. J Geophys Res 106:21843–21857

Narain H, Gupta HK (1968) Koyna earthquake. Nature 217:1138–1139

Nippress SEJ, Rietbrock A (2007) Seismogenic zone high permeability in the Central Andes inferred from relocations of micro-earthquakes. Eath Planet Sci Lett 263:235–245. doi:10.1016/j.epsl.2007.08.032

Obara K (2002) Nonvolcanic deep tremor associated with subduction in southwest Japan. Science 296:1679–1681. doi:10.1126/science.1070378

Obara K, Ito Y (2005) Very low frequency earthquakes excited by the 2004 off the Kii Peninsula earthquakes: a dynamic deformation process in the large accretionary prism. Earth Planets Space 57:321–326

Ohtake M (1974) Seismic activity induced by water injection at Matsushiro, Japan. J Phys Earth 22:163–176

Okusawa T, Tsukahara H (2001) Origin of deep ground water in the Matsushiro earthquake swarm area. Zisin Ser II:241–253 (in Japanese with English abstract)

Ozawa S, Kaidzu M, Murakami M, Imakiire T, Hatanaka Y (2004) Coseismic and postseismic crustal deformation after the M_w 8 Tokachi-oki earthquake in Japan. Earth Planets Space 56:675–680

Pacchiani F, Lyon-Caen H (2010) Geometry and spatio-temporal evolution of the 2001 Agios Ioanis earthquake swarm (Corinth Rift, Greece). Geophys J Int 180:59–72. doi:10.1111/j.1365-246X.2009.04409.x

Parotidis M, Shapiro SA, Rothert E (2005) Evidence for triggering of the Vogtland swarms 2000 by pore pressure diffusion. J Geophys Res 110:B05S10. doi:10.1029/2004JB003267

Paterson MS, Wong TF (2005) Experimental rock deformation—the brittle field. Springer, Heidelberg

Peacock SM (1996) Thermal and petrologic structure of subduction zones. In: Bebout GE, Scholl DW, Kirby SH, Platt JP (eds) Subduction top to bottom (Geophys Monogr Ser 96). American Geophysical Union, Washington DC, pp 119–133

Peacock SM, Christensen NI, Bostock MG, Audet P (2011) High pore pressures and porosity at 35 km depth in the Cascadia subduction zone. Geology 39:471–474. doi:10.1130/G31649.1

Peltzer G, Rosen P, Rogez F, Hudnut, K (1998) Poroelastic rebound along the Landers 1992 earthquake surface rupture. J Geophys Res 103:30131–30145

Peng Z, Ben-Zion Y (2006) Temporal changes of shallow seismic velocity around the Karadere-Düzce branch of the north Anatolian fault and strong ground motion. Pure Appl Geophy 163:567–600. doi:10.1007/s00024-005-0034-6

Perfettini H, Avouac JP (2004) Postseismic relaxation driven by brittle creep: a possible mechanism to reconcile geodetic measurements and the decay rate of aftershocks, application to the Chi-Chi earthquake, Taiwan. J Geophys Res 109:B02304. doi:10.1029/2003JB002488

Raleigh CB, Healy JH, Bredehoeft JD (1976) An experiment in earthquake control at Rangely, Colorado. Science 191:1230–1237

Rogers G, Dragert H (2003) Episodic tremor and slip on the Cascadia subduction zone: the chatter of silent slip. Science 300:1942–1943

Roland E, McGuire JJ (2009) Earthquake swarms on transform faults. Geophys J Int 178: 1677–1690. doi:10.1111/j.1365-246X.2009.04214.x

Rutledge JT, Phillips WS (2003) Hydraulic stimulations of natural fracture as revealed by induced microearthquakes, Carthage Cotton valley gas field, east Texas. Geophysics 68:441–452. doi:10.1190/1.1567214

Rutledge JT, Phillips WS, Mayerhofer MJ (2004) Faulting induced by forced fluid injection and fluid flow forced by faulting: an interpretation of hydraulic-fracture microseismicity, Carthage Cotton Valley gas field, Texas. Bull Seismol Soc Amer 94:1817–1830

Scotti O, Cornet FH (1994) In-situ evidence for fluid-induced aseismic slip events along fault zones. Int J Rock Mech Min Sci 31:347–358

Segall P (1989) Earthquakes triggered by fluid extraction. Geology 17:942–946

Segall P, Rice JR (1995) Dilatancy, compaction, and slip instability of a fluid-infiltrated fault. J Geophys Res 100:22155–22171

Seno T (2009) Determination of the pore fluid pressure ratio at seismogenic megathrusts in subduction zones: implications for strength of asperities and Andean-type mountain building. J Geophys Res 114:B05405. doi:10.1029/2008JB005889

Seno T, Zhao D, Kobayashi Y, Nakamura M (2001) Dehydration of serpentinized slab mantle: Seismic evidence from southwest Japan. Earth Planets Space 53:861–871

Shapiro SA, Huenges E, Borm G (1997) Estimating the crust permeability from fluid-injection-induced seismic emission at the KTB site. Geophys J Int 131:F15–F18

Shapiro SA, Rothert E, Rath V, Rindschwentner J (2002) Characterization of fluid transport properties of reservoirs using induced microseismicity. Geophysics 67:212–220. doi:10.1190/1.1451597

Shelly DR (2015) Complexity of the deep San Andreas fault zone defined by cascading tremor. Nat Geosci 8:145–151. doi:10.1038/NGEO2335

Shelly DR, Beroza GC, Ide S, Nakamula S (2006) Low frequency earthquakes in Shikoku, Japan, and their relationship to episodic tremor and slip. Nature 442:188–191. doi:10.1038/nature04931

Shelly DR, Moran SC, Thelen WA (2013a) Evidence for fluid triggered slip in the 2009 Mount Rainier, Washington earthquake swarm. Geophys Res. Lett 40:1506–1512. doi:10.1002/grl50354

Shelly DR, Hill DP, Massin F, Farrell J, Smith RB, Taira T (2013b) A fluid-driven earthquake swarm on the margin of the Yellowstone caldera. J Geophys Res 118:4872–4886. doi:10.1002/jgrb.50362

Šílený J, Hill DP, Eisner L, Cornet FH (2009) Non-double-couple mechanisms of micro-earthquakes induced by hydraulic fracturing. J Geophys Res 114:B08307. doi:10.1029/2008JB005987

Simpson DW (1986) Triggered earthquakes. Ann Rev Planet Sci 14:21–42

Suzuki T, Yamashita T (2010) Nondimensional control parameters governing the behavior of 1-D fault slip: effects of shear heating, inelastic pore creation and fluid flow. J Geophys Res 115: B02303. doi:10.1029/2009JB006557

Suzuki T, Yamashita T (2014) Effects of shear heating, slip-induced dilatancy and fluid flow on diversity of 1-D dynamic earthquake slip. J Geophys Res 119:2100–2120. doi:10.1002/2013JB010871

Tadokoro K, Ando M, Nishigami K (2000) Induced earthquakes accompanying the water injection experiment at the Nojima fault zone, Japan: seismicity and its migration. J Geophys Res 105:6089–6104

Taira T, Smith RB, Chang WL (2010) Seismic evidence for dilatational source deformations accompanying the 2004–2008 Yellowstone accelerated uplift episode. J Geophys Res 115: B02301. doi:10.1029/2008JB006281

Takada Y, Furuya M (2010) Aseismic slip during the 1996 earthquake swarm in and around the Onikobe geothermal area, NE Japan. Earth Planet Sci Lett 290:302–310. doi:10.1016/j.epsl.2009.12.024

Takei Y (2000) Acoustic properties of partially molten media studied on a simple binary system with a controllable dihedral angle. J Geophys Res 105:16665–16682

Takei Y (2002) Effect of pore geometry on V_P/V_S: from equilibrium geometry to crack. J Geophys Res 107:2043. doi:10.1029/2001JB000522

Tanaka Y, Kato A, Sugano T, Fu G, Zhang X, Furuya M, Sun W, Okubo S, Matsumoto S, Honda M, Sugawara Y, Ueda I, Kusaka M, Ishihara M (2010) Gravity changes observed between 2004 and 2009 near the Tokai slow-slip area and prospects for detecting fluid flow during future slow-slip events. Earth Planets Space 62:905–913. doi:10.5047/eps.2010.11.003

Terakawa T, Miller SA, Deichmann N (2012) High fluid pressure and triggered earthquakes in the enhanced geothermal system in Basel, Switzerland. J Geophys Res 117:B07305. doi:10.1029/2011JB008980

Toda S, Stein RS, Sagiya T (2002) Evidence from the AD 2000 Izuislands earthquake swarm that stressing rate governs seismicity. Nature 419:58–61. doi:10.1038/nature00997

van der Elst NJ, Savage HM, Keranen KM, Abers GA (2013) Enhanced remote earthquake triggering at fluid-injection sites in the Midwestern United States. Science 341:164–167. doi:10.1126/science.1238948

Vidale JE, Li YG (2003) Damage to the shallow Landers fault from the nearby Hector Mine earthquake. Nature 421:524–526

Vidale JE, Boyle KL, Shearer PM (2006) Crustal earthquake bursts in California and Japan: their patterns and relation to volcanoes. Geophys Res Lett 33:L20313. doi:10.1029/2006GL027723

Waite GP, Smith RB Allen RM (2006) V_P and V_S structure of the Yellowstone hot spot: evidence for an upper mantle plume. J Geophys Res 111:B04303. doi:10.1029/2005JB003867

Wang Z, Zhao D, Mishra OP, Yamada A (2006) Structural heterogeneity and its implications for the low frequency tremors in Southwest Japan. Earth Planet Sci Lett 251:66–78. doi:10.1016/j.epsl.2006.08.025

Wei S, Avouac JP, Hudnut KW, Donnellan A, Parker JW, Graves RW, Helmberger D, Fielding E, Liu Z, Cappa F, Eneva M (2015) The 2012 Brawley swarm triggered by injection-induced aseismic slip. Earth Planet Sci Lett 422:115–125. doi:10.1016/j.epsl.2015.03.054

Wicks C, Thelen W, Weaver C, Gomberg J, Rohay A, Bodin P (2011) InSAR observations of aseismic slip associated with an earthquake swarm in the Columbia River flood basalts. J Geophys Res 116:B12304. doi:10.1029/2011JB008433

Yamashita T (1999) Pore creation due to fault slip in a fluid-permeated fault zone and its effect on seismicity. Pure appl Geophys 155:625–647. doi:10.1007/s000240050280

Yamashita T (2013) Generation of slow slip coupled with tremor due to fluid flow along a fault. Geophys J Int 193:375–393. doi:10.1093/gji/ggs117

Yeo IW, De Freitas MH, Zimmerman RW (1998) Effect of shear displacement on the aperture and permeability of a rock fracture. Int J Rock Mech Min Sci 35:1051–1070

Yukutake Y, Honda R, Harada M, Aketagawa T, Ito H, Yoshida A (2011a) Remotely-triggered seismicity in the Hakone volcano following the 2011 off the Pacific coast of Tohoku Earthquake. Earth Planets Space 63:737–740. doi:10.5047/eps.2011.05.004

Yukutake Y, Ito H, Honda R, Harada M, Tanada T, Yoshida A (2011b) Fluid-induced swarm earthquake sequence revealed by precisely determined hypocenters and focal mechanisms in the 2009 activity at Hakone volcano. Japan. J Geophys Res 116:B04308. doi:10.1029/2010JB008036

Zhao D, Negishi H (1998) The 1995 Kobe earthquake: seismic image of the source zone and its implications for the rupture nucleation. J Geophys Res 103:9967–9986

Zhao D, Kanamori H, Negishi H, Wiens D (1996) Tomography of the source area of the 1995 Kobe earthquake: evidence for fluids at the hypocenter? Science 274:1891–1894

Zoback MD, Harjes HP (1997) Injection-induced earthquakes and crustal stress at 9-km depth at the KTB deep drilling site, Germany. J Geophys Res 102:18477–18491

http://www.springer.com/978-4-431-56560-4

Involvement of Fluids in Earthquake Ruptures
Field/Experimental Data and Modeling
Yamashita, T.; Tsutsumi, A.
2018, XIII, 187 p. 45 illus., 16 illus. in color., Hardcover
ISBN: 978-4-431-56560-4